G-band FMCW Radar for Humidity Profiling Inside Boundary Layer Clouds

Richard J. Roy, Ken B. Cooper, Matthew Lebsock, Luis Millán, Jose Siles, and Raquel Monje
Jet Propulsion Laboratory, California Institute of Technology
Pasadena, CA, USA

***Abstract*—We are developing a G-band FMCW radar for remote sensing of vertical water vapor profiles and total column water vapor. The radar utilizes the frequency-dependent absorption near the 183 GHz water absorption line to obtain a differential signal from which we can derive range-resolved humidity measurements. This proof-of-concept instrument will eventually be tested from an airborne platform. In this report, we discuss recent measurements and a humidity profile retrieval algorithm based on an absorption line shape fitting model.**

***Index Terms*—millimeter-wave radar, FMCW, differential absorption radar, humidity sounding**

I. Introduction

The water absorption line centered at 183 GHz is utilized by many passive remote sensing platforms to perform atmospheric humidity sounding, including the advanced microwave sounding unit (AMSU-B) and the humidity sounder for Brazil (HSB). However, these systems have limited ability to perform high-resolution observations of vertical water vapor profiles in the presence of clouds, contributing to deficiencies in numerical weather and climate change prediction capabilities [1, 2]. To fill this observational gap, we are currently developing a proof-of-concept FMCW radar instrument at 170 GHz to perform differential absorption radar (DAR) measurements from an airborne platform. This work leverages FMCW radar technology previously demonstrated at the Jet Propulsion Laboratory (JPL) at 675 GHz for security applications [3]. State-of-the-art components that maximize the radar sensitivity include high output power (> 500 mW) G-band frequency multipliers and InP low-noise amplifiers ($T_N = 500$ K).

By using a frequency-tunable transmitter that scans a flank of the 183 GHz absorption line, we can compare the relative absorption at different frequencies from in-cloud and surface radar echoes to retrieve range-resolved humidity profiles within clouds and total column water vapor. Numerical simulations utilizing high fidelity cloud models suggest that absolute humidity can be determined to within better than 25%. Here we present additional analysis of the DAR measurements described in [4], where now an absorption line shape fitting model for retrieving water vapor profiles is used, along with noise floor subtraction. These measurements were performed on the high-frequency flank of the water line ($183 - 193$ GHz). Ongoing work includes adapting the hardware to probe the low-frequency flank of the line around 170 GHz due to transmit frequency allocation restrictions between 174.8 and 191.8 GHz. An advantage of this lower frequency band is the possibility to penetrate lower into the atmosphere to measure boundary-layer water vapor.

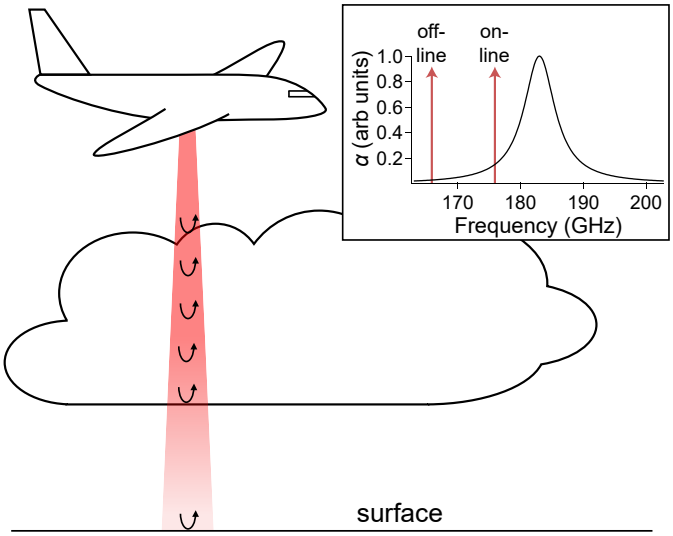

Fig. 1. Schematic of the airborne G-band DAR measurement concept. A nadir-pointing radar beam reflects off ice and liquid water particles in the cloud, as well as the Earth's surface.

II. Differential Absorption Radar Technique

The DAR measurement technique, an adaptation of the well-established differential absorption lidar (DIAL) method, has been previously demonstrated [4, 5]. Fig. 1 shows a schematic of how this technique can be implemented to retrieve in-cloud and total column water vapor. In the vicinity of an absorption resonance, the power returned from a single radar range bin depends strongly on frequency due to gaseous absorption. Thus, assuming other scattering characteristics (e.g. particulate extinction) are independent of frequency within the relatively small bandwidth used for the differential measurement, one can determine the average water vapor content between two range bins by comparing power ratios at each frequency with the known absorption line shape.

More formally, we can write the signal power returned from a range r at frequency f as

$$P_S(r, f) = G(f)Z(r)r^{-2}e^{-2\alpha(r,f)}, \quad (1)$$

where $G(f)$ is the frequency-dependent gain of the system, $Z(r)$ describes how the strength of the radar reflectivity

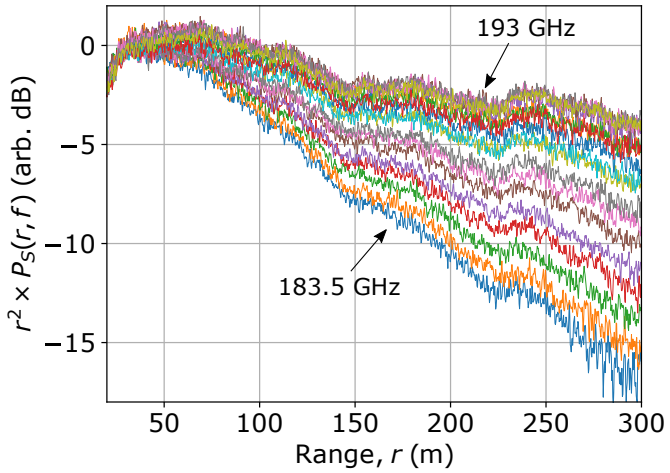

Fig. 2. FMCW signal power spectra scaled by the square of the range (see equation 1) to remove volumetric scattering effects. Each G-band frequency trace is normalized to its power at 30 m. The differential absorption is clearly seen by the dispersing of the lines with increasing range, with frequencies closer to the line center attenuating more strongly.

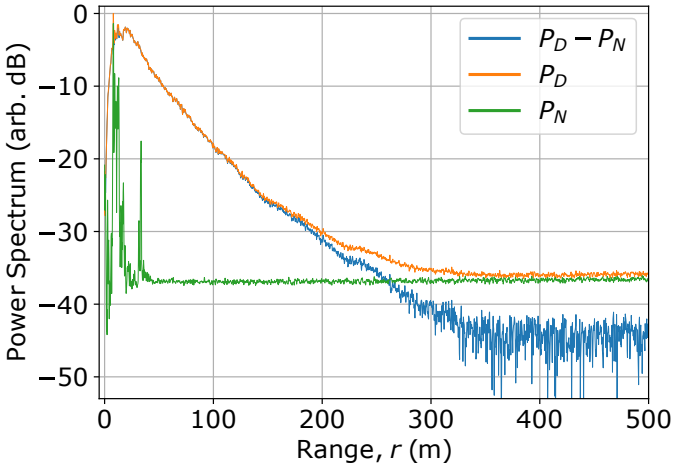

Fig. 3. Noise floor subtraction at 183.5 GHz. The noise floor trace (green) is measured with the same radar configuration in the absence of clouds and rain. Without background noise subtraction, the signal power variance would remain artificially small at ranges where there are no radar echoes detected.

varies with range (e.g. due to changing hydrometeor size distributions), $\alpha(r, f)$ is the one-way integrated water vapor attenuation, and we explicitly include the volumetric scattering r^{-2} term [4]. As discussed above, we assume that Z is independent of frequency. Taking the power ratio between two ranges r_1 and r_2, we find

$$\frac{P_S(r_2, f)}{P_S(r_1, f)} = \frac{Z(r_2)}{Z(r_1)} \left(\frac{r_1}{r_2}\right)^2 e^{-2\beta(r_1, r_2, f)R}, \qquad (2)$$

where $R = r_2 - r_1$ and we define β, the average specific attenuation between the points r_1 and r_2 with units of inverse distance.

As a demonstration of the DAR technique, we elaborate on ground-based measurements published previously [4] that were obtained by probing the upper flank of the 183 GHz line in the presence of precipitation. For this dataset, we perform FMCW measurements at 19 equally spaced frequencies from 183.5 to 193 GHz, acquiring 500 measurements at each frequency. Fig. 2 displays the FMCW power spectra averaged over the 500 measurements, showing the strong dependence of attenuation on frequency. For this figure we plot the signal power $P_S(r, f)$ times r^2, resulting in an FMCW spectrum that reveals the structure of the quantity $Z(r)\exp(-2\alpha(r, f))$ (see equation 1). In the earlier work, the FMCW spectra were analyzed to obtain the total attenuation over the full range where a radar signal from rain/clouds existed. Additionally, the analyzed range was restricted to the region where the signal-to-noise ratio (SNR) was high such that the background noise floor could be ignored in the analysis. In what follows, we partition the radar spectra in order to acquire range resolved humidity estimates, and account for the noise floor in order to extend the usable range beyond the high-SNR regime.

III. Water Vapor Profile Retrieval

In order to obtain reliable humidity values when the returned signal level is low, we must subtract the contribution to the FMCW spectrum from noise. To see why this is, we consider the case of a flat noise spectrum. Note that if we replace the power terms on the left hand side of equation 2 with the *detected* power P_D, the ratio of powers at two ranges for each frequency will approach unity for large ranges where the SNR is much less than one, leading us to conclude that there is zero attenuation (i.e. zero humidity). In fact, even at intermediate ranges where the signal power is comparable with the noise power, this effect would cause a systematic underestimate of the absorption between successive range bins.

To account for this, we begin by writing the detected power as $P_D = P_N + P_S$, where the noise power term P_N includes all contributions to the spectrum that do not result from clouds or rain signals. We measure P_D and P_N separately by waiting for the clouds and rain to clear before acquiring the background/noise power spectrum. Note that we cannot simply subtract a constant value for the noise spectral density (i.e. $k_B T_{\text{sys}}$) from the whole FMCW power spectrum to obtain P_S because of non-uniform gain characteristics throughout this band. Fig. 3 shows the spectra with and without noise floor cancellation, where the variance of $P_D - P_N$ begins diverging roughly 50 meters after crossing the noise level. The detected (orange) and signal (blue) power spectra begin deviating just before 200 meters range, indicating that regimes beyond this point would have yielded unreliable humidity estimates without noise floor subtraction.

The general protocol for retrieving the water vapor profile is depicted in Fig. 4a. After acquiring FMCW radar power spectra for $N = 19$ transmit frequencies, we choose a starting range r_1 and step size R with which to resolve the humidity profile. We then average the 500 measurements at each frequency for both cloudy (P_D) and clear-sky (P_N) conditions,

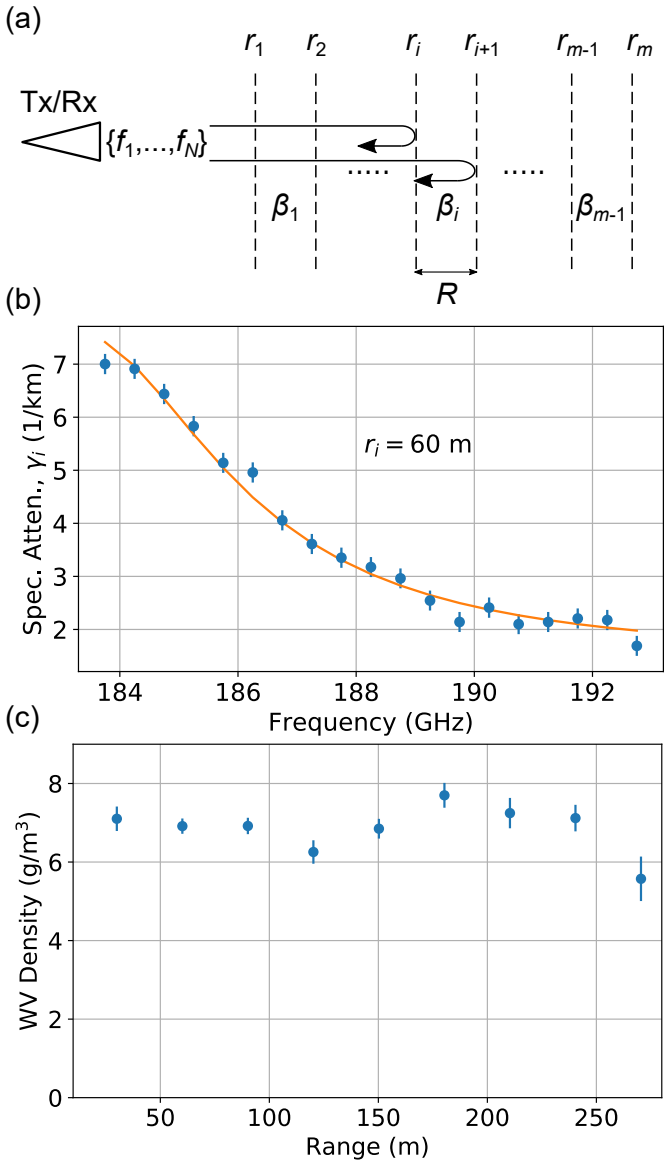

Fig. 4. (a) Protocol for retrieving profile by successively stepping in range by a distance R and performing fits to the absorption line shape (orange line in (b)). (b) Example of model fit to data at r_i = 60 m. (c) Retrieved water vapor (WV) density profile for measurements in Fig. 2.

keeping track of the standard error at each point in the spectrum. Then, after forming our estimate of $P_S = P_D - P_N$ and propagating the respective uncertainties, we compute for each r_i the frequency-dependent specific attenuation estimate,

$$\gamma_i(f_j) = \frac{1}{-2R} \ln \left[\left(\frac{r_{i+1}}{r_i} \right)^2 \frac{P_S(r_{i+1}, f_j)}{P_S(r_i, f_j)} \right]. \quad (3)$$

At each range bin r_i we average the points within a swath of ± 5 meters to increase precision in the estimate of $P_S(r_i, f_j)$. From equation 2, we see that $\gamma_i(f) = \beta_i(f) + C$, where C is constant containing information about the relative strength of scattering from the two range bins, and we define $\beta_i(f) = \beta(r_i, r_{i+1}, f)$. The measured G-band absorption spectrum (blue points in Fig. 4b) can then be fit with the known absorption line shape for each r_i, thus building up the water vapor profile as a function of range.

For these fits, we employ the same millimeter-wave propagation model as used in [6], and use atmospheric conditions as reported earlier in the day from a local weather station (286 K temperature and 1007 mbar pressure). The results are displayed in Fig. 4b and c. The two fitting parameters in this case are the water vapor (WV) density and the overall offset of the absorption line shape. The relative humidity (RH) range corresponding to the values in Fig. 4c is 60-70%, which is in slight disagreement with the value reported earlier in the day by the local weather station of 91%. However, the absorption line shape changes weakly with temperature, while the conversion from RH to WV density is exponential. Specifically, the average density obtained corresponds to 91% RH at 280 K, which is a reasonable temperature deviation to expect. The agreement between the measured absorption line shape and the model in Fig. 4b is very encouraging, and suggests that this fitting routine, which makes several simplifying assumptions as noted above, captures the relevant processes quite well.

IV. Conclusion

The method presented for retrieving water vapor profiles as a function of radar range using a DAR near the 183 GHz water line gives promising results using measurements on the high-frequency flank of the absorption line. This measurement technique is currently being adapted to probe the $167 - 174.8$ GHz frequency band, which is not subject to transmission restrictions, and offers the ability to penetrate further into a moist atmosphere, making possible remote sensing of boundary-layer water vapor. Important future studies include field testing with independent, coincident measurements of pressure, temperature, and RH from a radiosonde for instrument calibration, and eventually validation from an airborne platform.

Acknowledgment

The research was carried out at the Jet Propulsion Laboratory, California Institute of Technology, under a contract with the National Aeronautics and Space Administration. Copyright 2018 California Institute of Technology. U.S. Government sponsorship acknowledged.

References

[1] S. A. Buehler, M. Kuvatov, T. R. Sreerekha, V. O. John, B. Rydberg, P. Eriksson, and J. Notholt, "A cloud filtering method for microwave upper tropospheric humidity measurements," Atmos. Chem. Phys., vol. 7, pp. 5531-5542, 2007.

[2] T. J. Greenwald and S. A. Christopher, "Effect of cold clouds on satellite measurements near 183 GHz," Journal of Geophysical Research, vol. 107, no. D13, pp. AAC 3-1 3-8, 2002.

[3] K. B. Cooper, R. J. Dengler, N. Llombart, B. Thomas, G. Chattopadhyay, and P. H. Siegel, "THz imaging radar for standoff personnel screening," IEEE Transactions on Terahertz Science and Technology, vol. 1, no. 1, pp. 169-182, 2011.

[4] K. B. Cooper et al., "Atmospheric humidity sounding using differential absorption radar near 183 GHz," IEEE Geoscience and Remote Sensing Letters, vol. 15, no. 2, pp. 163-167, 2018.

[5] R. Lawrence et al., “Differential absorption microwave radar measurements for remote sensing of atmospheric pressure,” Geoscience and Remote Sensing Symposium, pp. 1045-1048, 2007.
[6] L. Millán, M. Lebsock, N. Livesey, and S. Tanelli, “Differential absorption radar techniques: water vapor retrievals,” Atmos. Meas. Tech., vol. 9, pp. 2633-2646, 2016.